Catalysis Today 164 (2011) 227–233

Contents lists available at ScienceDirect

Catalysis Today

journal homepage: www.elsevier.com/locate/cattod

Dry reforming of methane over $LnFe_{0.7}Ni_{0.3}O_{3-\delta}$ perovskites: Influence of Ln nature

L. Kapokova[a], S. Pavlova[a,*], R. Bunina[a], G. Alikina[a], T. Krieger[a], A. Ishchenko[a], V. Rogov[a], V. Sadykov[a,b]

[a] Boreskov Institute of catalysis, Novosibirsk, 630090, Russia
[b] Novosibirsk State University, Novosibirsk, 630090, Russia

ARTICLE INFO

Article history:
Received 30 June 2010
Received in revised form 23 October 2010
Accepted 26 October 2010
Available online 10 December 2010

Keywords:
Methane dry reforming
Ni–Fe perovskites
La
Pr
Sm substitution
Ni–Fe alloy

ABSTRACT

$LnFe_{0.7}Ni_{0.3}O_{3-\delta}$ (Ln = La, Pr, Sm) perovskites synthesized via Pechini method have been studied as catalysts of methane dry reforming (MDR). Effects of pretreatment and type of Ln cation on the structural and redox properties of perovskites and their catalytic performance have been elucidated. The most active catalysts are obtained by keeping perovskites in the reaction feed at high temperatures due to the formation of Ni–Fe alloy particles released from the perovskite lattice and stabilized on its surface. $PrFe_{0.7}Ni_{0.3}O_{3-\delta}$ was found to be the most active and stable catalyst due to the optimal composition of segregated Ni–Fe alloy particles and redox properties of oxide matrix.

1. Introduction

Recently, methane dry reforming (MDR) has attracted considerable attention as a process generating synthesis gas with the H_2/CO ratio close to unity which is a favorable feedstock for the production of oxygenates and liquid hydrocarbons in the Fischer–Tropsch synthesis [1].

The Ni-containing catalysts possessing a high initial activity are promising for the practical application due to their low cost. The drawbacks of these catalysts are sintering of nickel and their heavy coking. The solution of these problems is the incorporation of nickel in the oxide matrix with a high oxygen mobility such as CeO_2–ZrO_2 [2], perovskites of ABO_3 [3–10] or A_2BO_4 [11,12] types. This provides a high dispersion of the metal nickel formed under the reaction conditions and participation of oxide matrix oxygen in the reaction that prevents the catalyst coking and increases its activity and stability [7–9]. The oxygen mobility of perovskites could be adjusted by the substitution of A-site cation that allows tuning their catalytic performance in methane DR [6–10].

In this work results on the structural, redox and methane DR catalytic characterization of $Ln^1_{1-y}Ln^2_yFe_{0.7}Ni_{0.3}O_{3-\delta}$ (Ln = La, Pr, Sm; y = 0–0.1) perovskites (LnFN) are presented. The impact of the nature of cations in the A-site of perovskites on their real structure, redox properties and catalytic activity has been elucidated. For comparison, the MDR activity of PrO_x-supported Ni–Fe catalysts has been studied as well.

2. Experimental

Perovskites and praseodium oxide (PrO_x(P)) were synthesized by Pechini route using metal (Me) nitrates, citric acid (CA), ethylene glycol (EG) and ethylenediamine (ED) as reagents [13,14]. The molar ratio of CA:EG:ED:Me was 3.75:11.25:3.75:1. CA and metal nitrates were dissolved in ethylene glycol at 80 °C and in distilled water at room temperature, respectively. The prepared solutions were mixed together at room temperature under stirring followed by addition of ED. The prepared solution was stirred for 60 min and then heated at 70 °C for 24 h allowing for the gel formation. The gel was calcined at 600 °C for 2 h then obtained solids were ground and annealed at 900 °C. Praseodium oxide (PrO_x(n)) was also prepared by decomposition of nitrate salt under air followed by calcination at 900 °C. The supported catalysts (Ni,Fe)/PrO_x were prepared by incipient wetness impregnation of PrO_x with the mixed water solution of nitrates followed by calcination at 900 °C. The total content of Ni–Fe was 3, 5 and 7 wt% with the atomic ratio Ni/Fe = 4.

The samples of perovskites were characterized by XRD, BET, TEM with EDX, H_2 and CH_4 temperature-programmed reduction, O_2 temperature programmed desorption. The X-ray phase anal-

* Corresponding author. Tel.: +7 383 326 95 11; fax: +7 383 330 80 56.
E-mail address: pavlova@catalysis.ru (S. Pavlova).

0920-5861/$ – see front matter © 2010 Elsevier B.V. All rights reserved.
doi:10.1016/j.cattod.2010.10.086

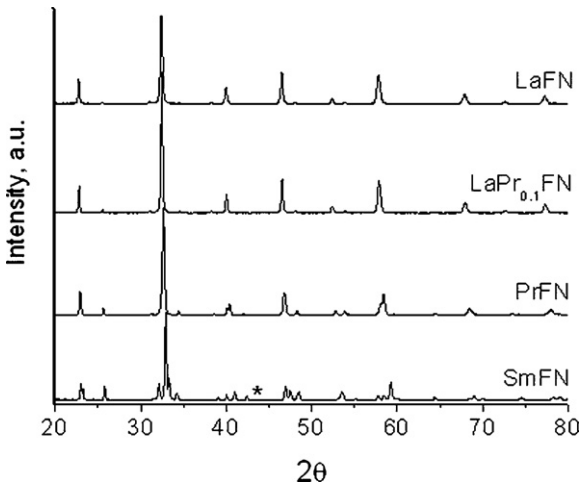

Fig. 1. XRD patterns of initial perovskites $LnFe_{0.7}Ni_{0.3}O_{3-\delta}$ calcined at 900 °C: NiO (*).

ysis of samples was carried out using ARLX·TRA diffractometer (Thermo, Switzerland) with CuKα radiation in the range of 2θ angles equal to 15–90°. BET specific surface area (SSA, m^2/g) was determined from the data on Ar thermodesorption. The TEM micrographs were obtained with a JEM-2010 instrument (lattice resolution 1.4 Å) and acceleration voltage 200 kV. Local elemental analysis was performed with EDX method (a Phoenix Spectrometer). The surface/bulk oxygen mobility for samples pretreated in O_2 at 500 °C was characterized by the temperature-programmed desorption (TPD) in He flow. The X-ray particle sizes were estimated by using the Scherrer equation.

Reactivity of perovskites was studied using temperature-programmed reduction (TPR) by H_2 (10% H_2 in Ar, feed rate 2.5 L/h, temperature ramp from 25 to 900 °C at 10°/min) or CH_4 (1% CH_4 in He, feed rate 10 L/h, temperature ramp from 25 to 880 °C at 5°/min). The experiments were carried out in kinetic installations equipped with GC Tcvet-500 and PEM-2 M analyzer (IR absorbance and electrochemical gas sensors).

The dry reforming reaction was carried out over the preoxidized or prereduced catalysts. The reaction was studied in the temperature-programmed mode (1% CH_4 + 1% CO_2 in He, contact time 0.005 s) as well as in steady-state conditions (10%CH_4 + 10% CO_2 in He, contact time 0.01 s) at temperatures up to 800–850 °C in a flow installation. To compare specific (per the surface unit) catalytic activity of different samples, effective first-order rate constants were calculated for the plug-flow reactors [15]. The long-term testing was performed in the reaction mixture 50% CH_4 + 50% CO_2 at 800 °C and contact time 0.1 s.

3. Results and discussion

3.1. Structural and textural features

Characteristics of initial perovskites and PrO_x-supported catalysts are presented in Tables 1 and 2. The BET specific surface areas of samples are in the range of 4–5 m^2/g which are comparable with the usual values obtained for such systems [8,16,17].

According to XRD data (Table 1, Fig. 1), all initial LnFN samples are single phase orthorhombic perovskites, the lattice parameters being close to known values [18,19], and only SmFN sample contains a trace admixture of NiO. The observed difference in the lattice parameters is due to the difference in the size of Ln cations (Table 1). For SmFN, splitting of reflections is observed due to the cooperative lattice distortion (Fig. 1). A similar phenomenon was earlier observed for $SmFeO_3$ perovskite and explained by a strong distortion of Sm-oxygen polyhedra, distortion of the Fe–O octahedra being small [19]. The average X-ray particle size for all perovskites was estimated to be ~100 nm.

After reduction at 600 °C in H_2, perovskites retain their structure but some shift of all reflections towards lower angles is observed showing the unit cell expansion due to reduction of Fe^{4+} and Ni^{3+} ions to larger Fe^{3+} and Ni^{2+} cations [19]. The XRD patterns of perovskites reduced in H_2 at 800 °C are presented in Fig. 2. For all samples, the observed phases are Ni–Fe alloy, remaining perovskites with changed parameters and La_2O_3, Pr_2O_3 or Sm_2O_3 depending on the composition of starting samples. The lattice parameter of Ni–Fe alloy (Table 1) changes with the Ln cation nature but in all cases it is intermediate between those of pure metal Ni face-centered cubic lattice – 3.5240 Å [JCPDF 65-2865] and $Fe_{0.64}Ni_{0.36}$ alloy – 3.5922 Å [JCPDF 47-1405]. For the LaFN and LaPrFN precursors, the Ni–Fe alloy composition is close (Table 1) while for PrFN, a larger parameter indicates that the alloy is highly enriched by Fe. The X-ray alloy particle size is smaller for Pr-containing samples.

The structure of praseodymium oxides prepared both by nitrate decomposition and via Pecini method corresponds to that of $Pr_{12}O_{22}$ [JCPDF 89-573]. The XRD patterns of (Ni,Fe)/PrO_x supported catalysts along with reflections of $Pr_{12}O_{22}$ show weak peaks corresponding to $PrNiO_3$ perovskite [JCPDF 79-2455]. Some shift of perovskite reflections with respect to those of stoichiometric $PrNiO_3$ is observed due to apparent Fe incorporation into the perovskite structure.

3.2. H_2 TPR

The H_2 TPR profiles of all LnFN perovskites are presented in Fig. 3. In all cases, three main peaks are observed in the patterns: the intense low-temperature peak with the maximum at 317–354 °C, the low intensity peak at 386–445 °C and unresolved intense high-temperature peak above 600 °C. The first low-temperature peak is assigned to reduction of Ni^{3+} to Ni^{2+}, and the second one corresponds to reduction of Fe^{4+} cations to Fe^{3+} state within the perovskite lattice that is in agreement with known results [9,16] and our XRD data showing retention of perovskite structure after reduction at 600 °C. The high-temperature peak is attributed to the partial destruction of perovskite structure with formation of Ni–Fe alloy and corresponding oxides (Fig. 2). In going from LaFN to SmFN, the low-temperature peaks are shifted to higher temperature while the high-temperature peaks are shifted to lower temperatures. The trend of increasing the temperature of a partial Ni^{3+} (Fe^{4+}) cations reduction in this order agrees with the data for $LaFeO_3$, $NdFeO_3$ and

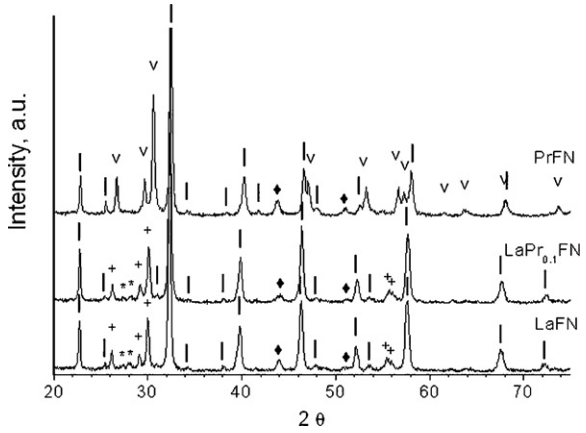

Fig. 2. XRD patterns of $LnFe_{0.7}Ni_{0.3}O_{3-\delta}$ perovskites reduced at 800 °C in H_2 (perovskite (|), La_2O_3 (+), Ni–Fe alloy (♦), $La(OH)_3$ (*), Pr_2O_3 (V)).

Table 1
Unit cell parameters, secondary phases and BET results for perovskites $LnFe_{0.7}Ni_{0.3}O_{3-\delta}$ with different Ln-cations calcined at 900 °C.

Ln	La	LaPr	Pr	Sm
Ionic radius* (Å)	1.36		1.31	1.24
a (Å)	5.511	5.500	5.522	5.572
b (Å)	7.808	7.809	7.742	7.657
c (Å)	5.537	5.462	5.462	5.376
V (Å^3)	238.25	237.39	233.54	229.34
Secondary phase	–	–	–	NiO
SSA (m^2/g)	4	4	4	5
D_{alloy}** (H_2, 800 °C) (Å)	175	115	160	–
Lattice parameter of alloy (H_2, 800 °C) (Å)	3.567	3.560	3.579	–

* R.D. Shannon, Acta Crystallogr., Sect. A 32 (1976) 751.
** X-ray particle size.

Table 2
Specific surface area of praseodymium oxides and supported Ni–Fe catalysts.

Sample	SSA (m^2/g)
$Pr_xO_y(n)$	2.3
Pr_xO_y(P)	3.7
3% Ni–Fe/$Pr_xO_y(n)$	5.2
5% Ni–Fe/Pr_xO_y(P)	4
7% Ni–Fe/Pr_xO_y(P)	4

$SmFeO_3$ reported in [17,19]. Such a trend has been explained by the decrease of the Fe–O bond distances from $LaFeO_3$ to $SmFeO_3$ estimated from the cell size and, thus, by the increase of the Fe–O bond strength. Since for $LnFe_{0.7}Ni_{0.3}O_3$ the cell volume also decreases in the order from La to Sm (Table 1), it is reasonable to suppose the same reason for more difficult reduction of $Ni^{3+}(Fe^{4+})$ cations for SmFN perovskite. The shift of high-temperature peak to lower temperatures is determined by the decrease of perovskite lattice stability in going from LaFN to SmFN. LaFN and PrFN having less disordered structures are more stable to reduction as compared with SmFN perovskite (Fig. 1) with the most distorted Sm–O polyhedra [19].

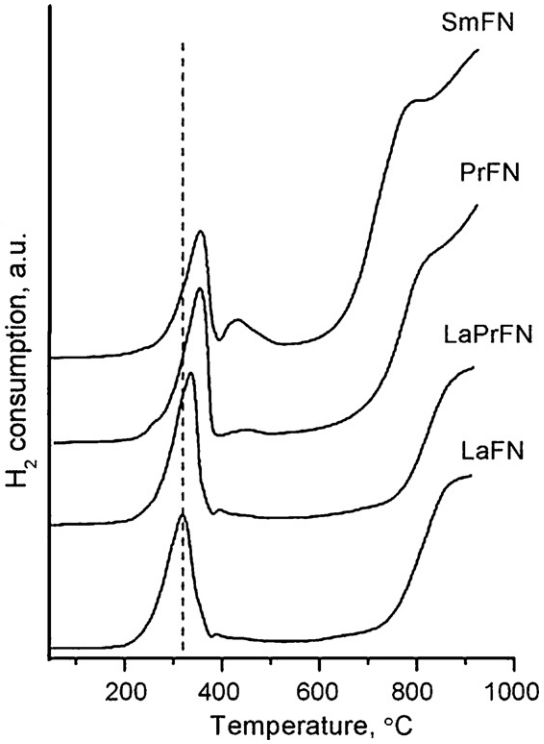

Fig. 3. H_2-TPR profiles for the $LnFe_{0.7}Ni_{0.3}O_{3-\delta}$ perovskites.

3.3. CH_4 TPR

Temperature-programmed reduction of perovskites by methane usually proceeds at higher temperatures as compared with the reduction by H_2 due to a strong C–H bond in CH_4 molecule. Typical profiles of the CH4 and product concentration variation during TPR for PrFN perovskite are presented in Fig. 4. Reduction starts by formation of deep oxidation products (H_2O and CO_2) at 480–540 °C as a result of interaction of activated CH_x species with highly reactive surface oxygen. At 620–700 °C, CO and H_2 start to evolve due to interaction with strongly bound surface oxygen replenished by the lattice oxygen migration from the bulk of particles. These peaks along with a peak of CO_2 evolution are situated at 700–850 °C (Figs. 4 and 5). The complete reduction of perovskite proceeds with the formation of Fe–Ni alloy and corresponding Ln oxide that is confirmed by XRD (not shown for brevity). The temperature of maximal rates of the product formation and their values for all LnFN perovskites are presented in Fig. 5. The relation among the rates of products formation evidently changes with the nature of Ln cation determining reactivity and mobility of the surface/bulk oxygen of perovskites.

3.4. Methane dry reforming

Typical profiles of products concentration variation during MDR temperature-programmed reaction are shown in Figs. 6 and 7. For all perovskites, the consumption of CH_4 and CO_2 starting at 600–650 °C is followed by the formation of CO while hydrogen appears at higher temperatures (Figs. 6 and 8). Such a sequence of products formation could be explained by occurring reverse water

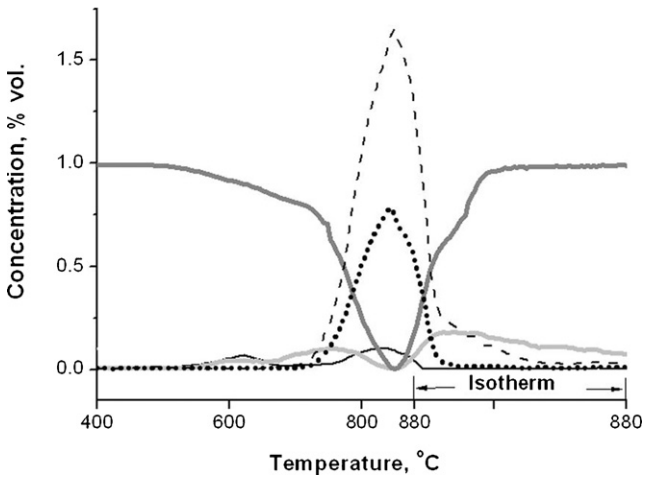

Fig. 4. The variation of CH_4 and product concentration during CH_4-temperature-programmed reduction of PrFN: ( ) CH_4, (—) CO_2, (···) CO, (- - -) H_2, ( ) H_2O.

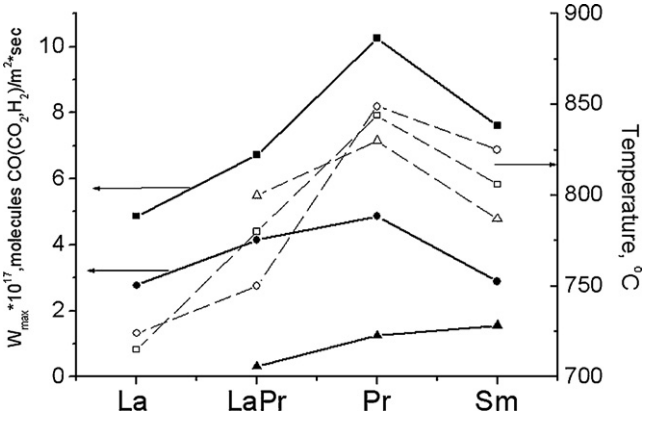

Fig. 5. Temperature-programmed reduction of $LnFe_{0.7}Ni_{0.3}O_{3-\delta}$ perovskites with CH_4: maximal rates of H_2 (■), CO (●) and CO_2 (▲) formation and temperatures of corresponding maxima (H_2 (□), CO (○) and CO_2 (△) respectively).

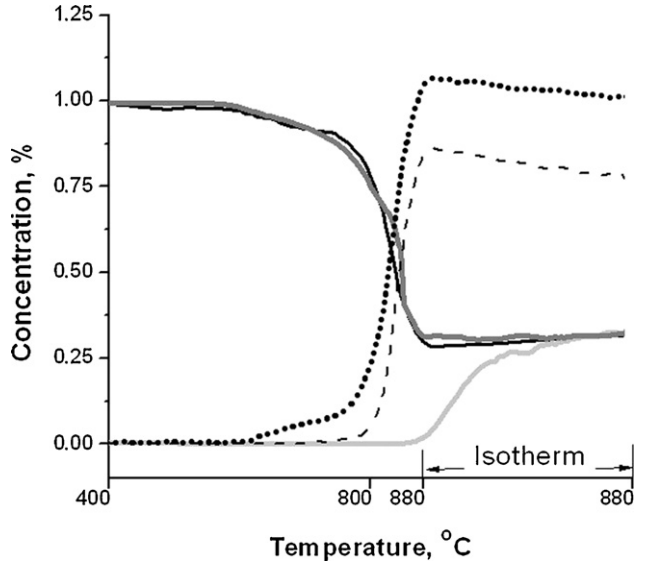

Fig. 6. Typical curves of reagents and products concentration variation in the temperature-programmed reaction of CH_4 dry reforming for PrFN catalyst pretreated in O_2. Contact time 5 ms, feed 1% CH_4 + 1%CO_2 in He. (▬) CH_4, (—) CO_2, (···) CO, (- - -) H_2, (▬) H_2O.

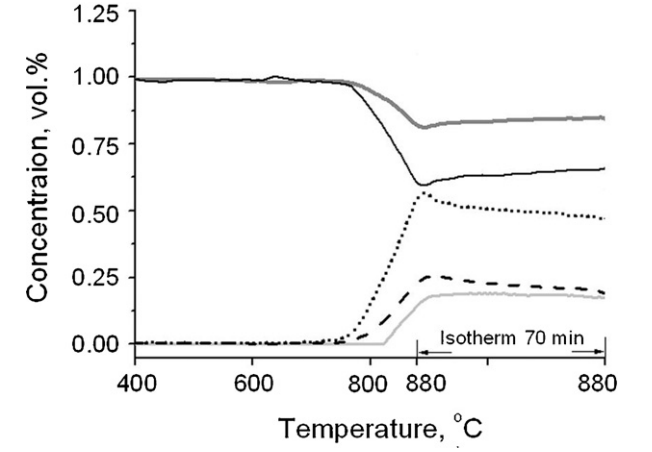

Fig. 7. Typical curves of reagents and products concentration variation in the temperature-programmed reaction of CH_4 dry reforming for 3% Ni–Fe/Pr_xO_y(*n*) catalyst pretreated in O_2. Contact time 5 ms, feed 1% CH_4 + 1%CO_2 in He. (▬) CH_4, (—) CO_2, (···) CO, (- - -) H_2, (▬) H_2O.

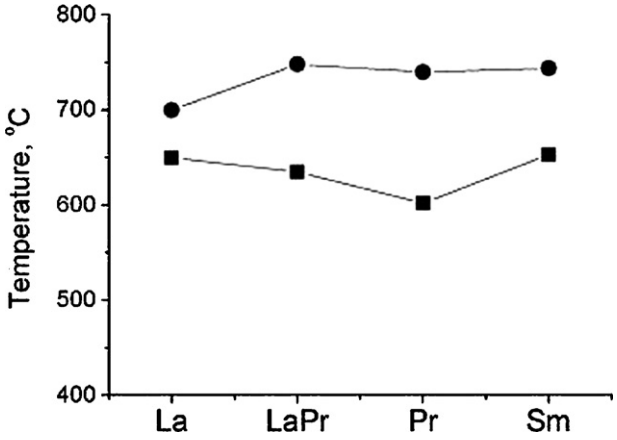

Fig. 8. Starting temperature of products formation during the temperature-programmed reaction of CH_4 dry reforming for LnFN perovskites: (●) H_2, (■) CO.

gas shift reaction (RWGS) at temperature below 700 °C. Note, that while the starting temperature of H_2 formation is lower for LaFN and is practically the same for other perovskites, CO appears at the lowest temperatures for Pr-containing perovskites. Hence, the nature of Ln cation in perovskite affects selectivity of CH_4 transformation into products, perhaps, via different share of RWGS reaction.

In the case of 3%(Ni,Fe)/PrO_x catalyst, formation of CO and H_2 starts at nearly the same temperatures ~740 and 750 °C, respectively (Fig. 7), which are higher as compared with those for PFN catalyst (Fig. 6). Furthermore, the methane and CO_2 conversions are quite low and different ~13% and 35%, respectively, while for PFN they are much higher (~70%) and close to each other. Hence, for 3%(Ni,Fe)/PrO_x catalyst, a higher CO_2 conversion and a low value of H_2/CO ratio (0.4) show a significant impact of RWGS reaction.

The steady-state catalytic characteristics in the reaction feed 10% CH_4 + 10% CO_2 in He also demonstrated a higher activity of PFN catalyst as compared with supported catalysts 5(7)%(Ni,Fe)/PrO_x: for PFN catalyst, the effective first-order rate constant is one order of magnitude higher (Table 3). Thus, perovskite as the catalyst precursor provides a higher specific activity in MDR.

Ni-containing perovskites are well known to be good precursors of active MDR catalysts comprised of dispersed metal nickel particles located in the oxide matrix [4–10]. The formation of such nanocomposites either requires reductive pretreatment of starting perovskites or it occurs directly in the reaction media [8,20]. To study the effect of pretreatment on the catalyst activity, all initial LnFN perovskites were activated in the reaction mixture at 850 °C or in the H_2 flow at 600 °C (only PrFN at 800 °C as well) before the catalytic tests.

The temperature dependence of methane conversion for all perovskites activated and tested in the reaction mixture containing 10%CH_4 + 10%CO_2 are presented in Fig. 9. The values of methane conversions at 800 °C for perovskites activated in the reaction mixture and in the flow of H_2 at 600 °C are shown in Fig. 10. Among the samples activated in the reaction mixture, the conversion values decrease in the order PrFN > LaPrFN, SmFN > LFN (Figs. 9 and 10). A low methane conversion over LFN perovskite could be explained by its difficult reduction as shown by H_2 TPR (Fig. 3). Indeed, pre-reduction of LaFN and LaPrFN at 600 °C in H_2 leads to a higher

Table 3
Rate constants of MDR at 800 °C.

Catalyst	K (m^{-2} s^{-1})
PFN	15
5% Ni–Fe/Pr_xO_y(P)	1.1
7% Ni–Fe/Pr_xO_y(P)	1.2

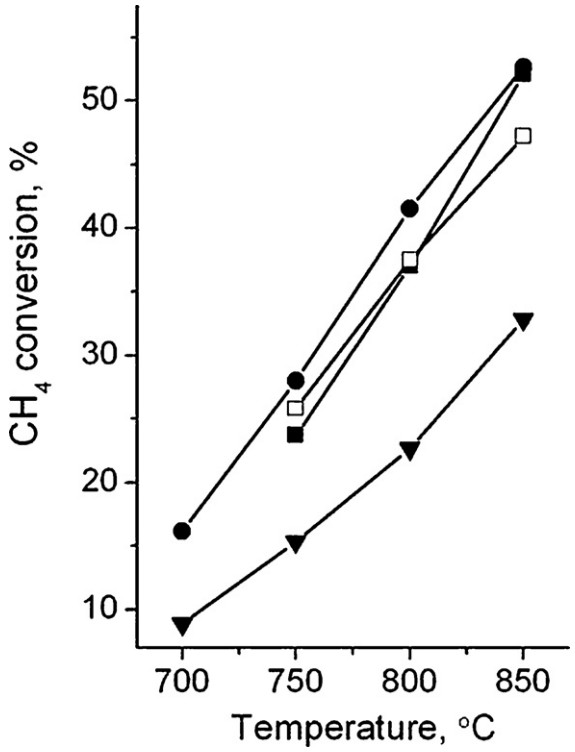

Fig. 9. Temperature dependence of methane conversion in MDR over the $LnFe_{0.7}Ni_{0.3}O_{3-\delta}$ (Ln = La (▼), LaPr (■), Pr (●), Sm (□)) activated in the reaction mixture. The feed 10%CH_4 + 10%CO_2, He-balance, contact time 0.01 s.

methane conversion (Fig. 10). At the same time, the reduction of PrFN at 800 °C in H_2 leads to a lower activity (Fig. 11) as compared to samples activated in the reaction mixture or reduced at 600° that is determined by the destruction of perovskite with the formation of alloy enriched with Fe as shown by XRD data (Fig. 2). The results of long-term testing of PrFN catalyst activated in the concentrated feed (CH_4:CO_2 = 1:1) show its high activity and stability (Fig. 12).

The comparison of methane conversion values for perovskites reduced in H_2 and activated in the reaction mixture shows that only in the case of PrFN they are close while for all other samples conversions differ noticeably. Such a difference in the activity appears to be determined by the composition of the active Ni–Fe alloy particles formed in the oxide matrix depending on reducing media and the type of Ln cation in perovskite. Indeed, the XRD data show that,

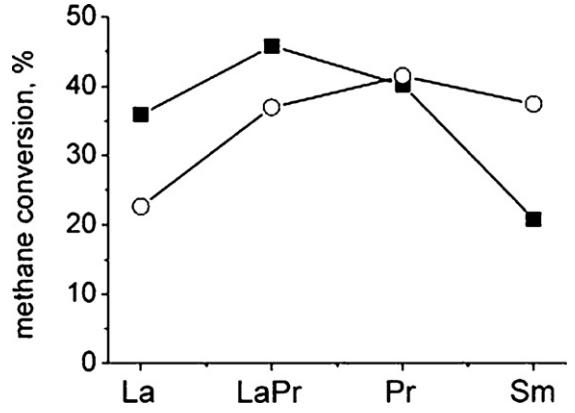

Fig. 10. Methane conversion in CH_4 dry reforming over $LnFe_{0.7}Ni_{0.3}O_{3-\delta}$ (Ln = La, LaPr, Pr, Sm) reduced at 600 °C in H_2 (■) or activated in the reaction mixture (○). The feed 10%CH_4 + 10%CO_2, He-balance, 800 °C, contact time—0.01 s.

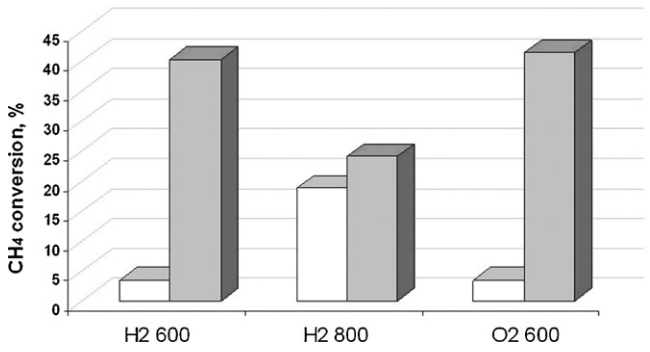

Fig. 11. Initial (□) and steady-state (■) conversion of methane over PrFN oxidized at 600° in O_2 and reduced in H_2 at 600 and 800 °C. The feed 10%CH_4 + 10%CO_2, He-balance, 800 °C.

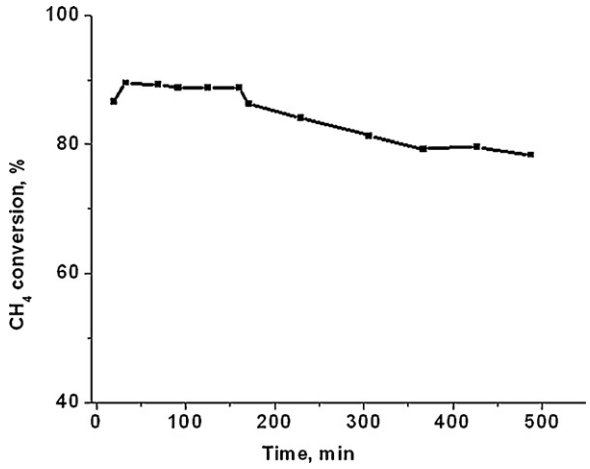

Fig. 12. The long-term test of PrFN activated in the reaction mixture. The feed: 50%CH_4 + 50%CO_2, 800 °C, 0.1 s.

in the case of PrFN, Ni–Fe alloy with a higher Fe content is formed after reduction in H_2 at 800 °C Fig. 13. (Table 1, Fig. 2).

It is known that activity and coking stability of Ni-containing catalysts are controlled by the ensemble effect when, for reforming reaction, the ensemble of Ni atoms is smaller than that for nucleation of carbon whiskers [21]. Therefore, a higher dilution of metal Ni with Fe favors a higher activity and stability of the catalyst formed from PrFN as compared with LaFN and LaPrFN. At the same time, a higher activity of catalysts activated in the reaction mixture could be conditioned by the optimal composition of

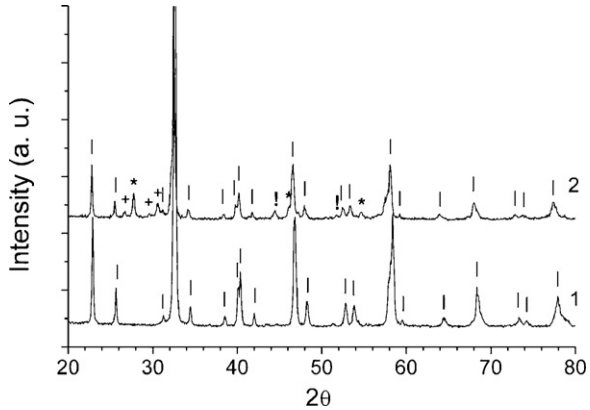

Fig. 13. XRD patterns of perovskite $PrFe_{0.7}Ni_{0.3}O_{3-\delta}$: initial (1) and used (2): perovskite (|), Pr_2O_3 (+), Pr_nO_{2n+2} (*), Ni–Fe alloy (!).

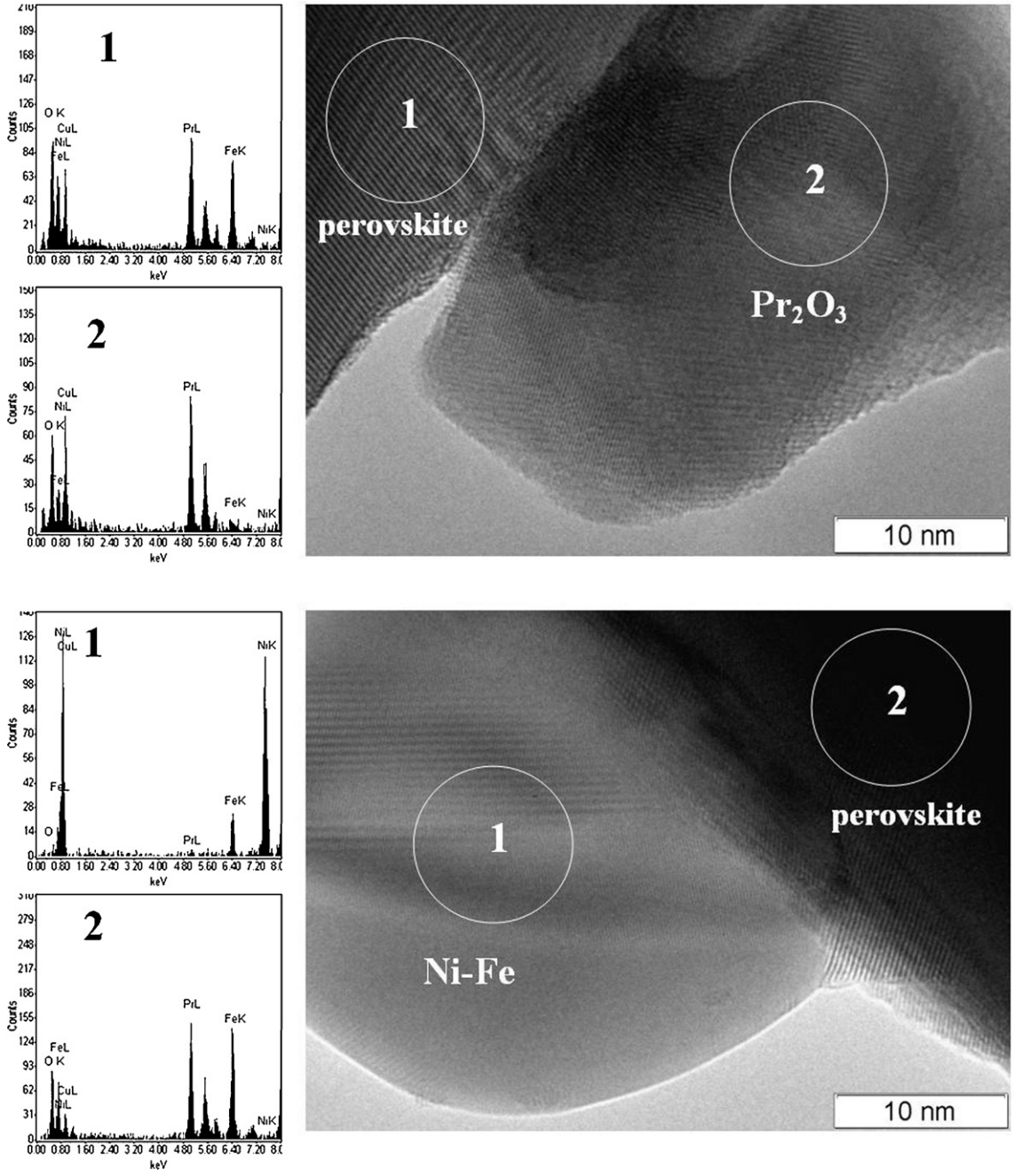

Fig. 14. High-resolution TEM image of used PrFN0.3 catalyst with EDX: (a) 1 – perovskite, 2 – Pr_xO_y; (b) 1 – Ni–Fe alloy, 2 – perovskite.

Ni–Fe alloy. Furthermore, if activation of methane is determined by the metallic phase, activation of CO_2 occurs with the participation of the oxide matrix and could be governed by its redox properties. The data of oxygen thermodesorption show the maximal rate of oxygen desorption at high temperature for PrFN as compared with other perovskites (Table 4). Probably, praseodymium oxides possessing a high redox activity [7] may react with CO_2 and with carbon residues thus facilitating reforming reaction and preventing catalyst coking. However, it is not sufficient to provide a high and stable performance of Ni–Fe alloy particles as clearly demonstrated by much lower activity of PrO_x-supported catalysts as compared with those derived from perovskite precursors (Table 3). Hence, perovskite phase remaining even after prolonged contact of catalysts with concentrated feed (CH_4:CO_2 = 1:1) at high temperatures (Figs. 14 and 15) appears to be the most important factor providing a high and stable performance. This can be explained by a high reactivity and mobility of the surface/lattice oxygen of these ferrite-type perovskites disordered due to reductive segregation of Ni (Fig. 14). This helps to provide an efficient route of CO_2 activation on the surface of perovskites and a fast transfer of oxygen atoms

Table 4
Data of O_2 TPD: desorption of bulk oxygen.

Sample	$W_{max} \times 10^{-14}$ (O_2 molecules/m^2 s)	T_{max} (°C)
$LP_{0.1}FN$	6	889
PFN	9	879
SFN	6	892

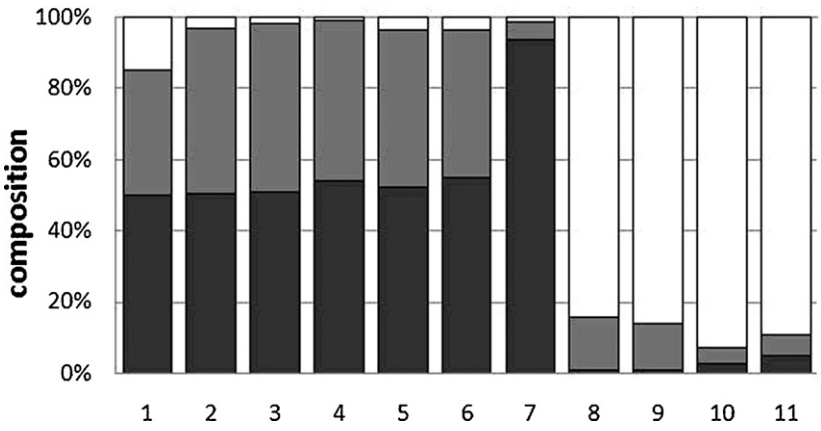

Fig. 15. EDX elemental distribution for $PrFe_{0.7}Ni_{0.3}O_{3-\delta}$-based catalyst after testing in the reaction mixture CH_4:CO_2 = 1:1. 1 – integral; 2–6 – perovskite particles; 7 – praseodimium oxide; 8–11 – Ni-Fe-alloy particles. Ni □, Fe ■, Pr ■.

or oxygen-containing species (hydroxyls, hydroxocarbonates, etc.) to the interface with segregated Ni–Fe alloy particles where they consume activated CH_x fragments–coke precursors.

Though composition of these alloy particles vary broadly (Fig. 15), neither coke deposits nor fibers were detected in discharged catalysts. This implies that a high lattice oxygen mobility and surface reactivity of nanostructured PrO_x/$LnFeO_y$ supports generated by reductive decomposition of complex perovskite precursors in the reaction media play more important role in preventing coking of supported Ni–Fe alloy particles than their exact chemical composition (Fe content).

4. Conclusion

In realistic conditions of CH_4 dry reforming $LnFe_{0.7}Ni_{0.3}O_{3-\delta}$ (Ln = La, Pr, Sm, Sr) perovskites are transformed onto composites comprised of Ni–Fe alloy particles and LnO_x epitaxially bound with Ln–Fe–O perovskite particles. The type of Ln cation affects both Fe content in alloy particles and oxygen mobility/reactivity in perovskites. Special experiments with PrO_x supported Ni–Fe alloy particles revealed their much lower activity as compared with composites obtained by reductive transformation of $LnFe_{0.7}Ni_{0.3}O_{3-\delta}$ precursors. This demonstrates an important role played by remaining Ln–Fe–O phase in composites in CH_4 dry reforming via activation of CO_2 and transfer of active oxygen-containing species to Ni–Fe alloy particles where they interact with CH_x fragments producing syngas. $PrFe_{0.7}Ni_{0.3}O_{3-\delta}$ has been shown to be the most active and stable catalyst due to optimal composition of formed Ni–Fe alloy and red-ox properties of oxide matrix.

Acknowledgements

Support by OCMOL FP7 Project, Project no. 57 of Presidium RAN Program 27, RFBR-CNRS 09-03-93112 and the Russian Federal Innovation Agency via the program “Scientific and Educational cadres” is gratefully acknowledged.

References

[1] Y.H. Hu, E. Ruckenstein, Adv. Catal. 48 (2004) 297.
[2] J.A. Montoya, E. Romero-Pascual, C. Gimon, P. Del Angel, A. Monzón, Catal. Today 63 (2000) 71.
[3] G.C. Araujo, S.M. Lima, J.M. Assaf, M.A. Pena, J.L.G. Fierro, M.C. Rangel, Catal. Today 133–135 (2008) 129.
[4] M.R. Goldwasser, M.E. Rivas, E. Pietri, M.J. Perez-Zurita, M.L. Cubeiro, L. Gingembre, L. Leclercq, G. Leclercq, Appl. Catal. A: Gen. 255 (2003) 45.
[5] J. Woo Nam, H. Chae, S. Ho Lee, H. Jung, K.-Y. Lee, Stud. Surf. Sci. Catal. 119 (1998) 843.
[6] G.S. Gallego, C. Batiot-Dupeyrat, J. Barrault, E. Florez, F. Mondragon, Appl. Catal. A: Gen. 334 (2008) 251–258.
[7] G.S. Gallego, J. Gallego Marín, C. Batiot-Dupeyrat, J. Barrault, F. Mondragon, Appl. Catal. A: Gen. 369 (2009) 97–103.
[8] H. Provendier, C. Petit, C. Estournes, A. Kiennemann, Stud. Surf. Sci. Catal. 119 (1998) 741.
[9] H. Provendier, C. Petit, C. Estournes, A. Kiennemann, Chemistry 4 (2001) 57.
[10] G. Valderrama, M.R. Goldwasser, C. Urbina de Navarro, J.M. Tatibouet, J. Barrault, C. Batiot-Dupeyrat, F. Martinez, Catal. Today 107–108 (2005) 785–791.
[11] G.S. Gallego, F. Mondragon, J. Barrault, J.-M. Tatibouët, C. Batiot-Dupeyrat, Appl. Catal. A: Gen. 311 (2006) 164–171.
[12] G.S. Gallego, F. Mondragon, J. Tatibouet, J. Barrault, C. Batiot-Dupeyrat, Catal. Today 133–135 (2008) 200–209.
[13] M.P. Pechini, US Patent 3, 330, 697 (1967).
[14] T.G. Kuznetsova, V.A. Sadykov, E.M. Moroz, S.N. Trukhan, E.A. Paukshtis, V.N. Kolomiichuk, E.B. Burgina, V.I. Zaikovskii, M.A. Fedotov, V.V. Lunin, E. Kemnitz, Stud. Surf. Sci. Catal. 143 (2002) 659.
[15] N.N. Sazonova, V.A. Sadykov, A.S. Bobin, S.A. Pokrovskaya, E.L. Gubanova, C. Mirodatos, React. Kinet. Catal. Lett. 98 (2009) 35.
[16] H. Falcon, J. Baranda, J.M. Campos-Martin, M.A. Pena, J.L.G. Fierro, Surf. Sci. Catal. 130 (2000) 2195.
[17] P. Ciambelli, S. Cimino, S. De Rossi, L. Lisi, G. Minelli, P. Porta, G. Russo, Appl. Catal. B: Environ. 29 (2001) 239.
[18] R. Kumar, R.J. Choudhary, M. Ikram, D.K. Shukla, S. Mollah, P. Thakur, K.H. Chae, B. Angadi, W.K. Choi, J. Appl. Phys. 102 (2007) 073707.
[19] P. Porta, S. Cimino, S. De Rossi, M. Faticanti, G. Minelli, I. Pettiti, Mater. Chem. Phys. 71 (2001) 165.
[20] J. Juan-Juan, M.C. Roman-Martinez, M.J. Illan-Gomez, Appl. Catal. A: Gen 355 (2009) 27.
[21] J.R. Rostrup Nielsen, Stud. Surf. Sci. Catal. 68 (1991) 85.